中國造船工程學刊第二期第143～158頁（民國七十二年十月）
Journal of the Society of Naval Architects and Marine Engineers, R. O. C.No. 2, PP. 143－158 (1983, 10)

利用縱向波形分析方法測量船舶興波阻力及其線上實驗系統

DETERMINATION OF SHIP WAVE-RESISTANCE BY THE LOGITUDINAL WAVE PATTERN ANALYSIS METHOD AND ITS ON-LINE EXPERIMENTAL SYSTEM

蔡武廷　林允進　廖清照
國立台灣大學　造船工程研究所　中正理工學院　工學部

摘　要

本文爲有關縱向波形分析理論與實驗之探討。由船舶興波邊界值問題之積分表示形式，對平行於船舶前進方向之波高或波高斜率取Fourier Transform，則可求得一縱向波高或波高斜率與船舶興波阻力間之關係，此即所謂Newman-Sharma 縱向波形分析理論。有關由於實驗水槽之有限寬度和長度，而需引用之截斷修正亦於文中討論。以此理論爲基礎，本文於國立台灣大學造船工程研究所之實驗水槽，建立了一套縱向波形分析之線上實驗系統，其實驗之控制、計測以及計算、分析皆利用一微計算機處理。實驗之結果包括一拋物線船型以及一驅逐艦船型。

Abstract

The experimental method, proposed by Newman (1963) and Sharma (1963, 1966), for the purpose of direct determination of steady ship wave-resistance from the measured longitudinal wave pattern is presented. This is known as the Newman-Sharma longitudinal wave pattern analysis method, based on the Fourier transform of the wave height or slope along a longitudinal cut parallel to path of the steadily moving ship. Correction for the trunction of the measured wave profile due to finite width and length of the towing basin is also discussed. An on-line experimental system based on such analysis method is established in the experimental towing tank of the Institute of Naval Architecture, the National Taiwan University. The control, measurement and computation of the experiment are all executed by a microcomputer. Two experimental results, one for a parabolic hull form and the other for a destroyer hull form, are presented.

Introduction

During the International Seminar on Theoretical Wave Resistance held at the University of Michigan in 1963, the problem dealing with the evaluation of wave resistance from direct measurement of the ship wave has attracted a great deal of attention. Among the methods proposed, the formulations based on measuring wave profile along a longitudinal cut parallel to ship's track offer the most simple experimental procedure. This method is known as the longitudinal wave-pattern analysis. Several authors, Newman (1963), Pien and Moore (1963), Sharma (1963) and Shor (1963), have presented different formulations concerned the longitudinal wave-pattern analysis method in that Seminar. The formulation introduced by Newman and that by Sharma are similar. They employed the technique of the Fourier transform to analyze the measured wave profile, and is usually known as the Newman-Sharma longitudinal-cut method.

In this paper the formulation of the longitudinal wave-pattern analysis is derived first, which follows the Newman's method but with a slight difference. A correlation of the longitudinal wave profile and the

wave resistance of a ship is obtained. Correction of the truncated wave profile due to the finite width and length of the towing tank is also discussed.

The main difficulty arising in the experiment of longitudinal wave-pattern analysis is the data acquisition, transformation and analysis. Accordingly, automation of the experiment is required to reduce the time for data arrangement, and to improve the accuracy of measurement and numerical computation. In the present experiment, a microcomputer is employed to control the measuring procedure and to execute the data arrangeement and analysis. The longitudinal wave-pattern analysis system established here is thus an on-line experimental system.

The experimental results for a parabolic hull form and that for a destroyer hull form are presented. The parabolic hull form, which is a simple wave-making mechanism, is used to verify the experimental system. For the destroyer hull form, a modified model with a bulbous bow and a stern-end-bulb is also implemented. Stern-end-bulb is a new idea which, like that of bulbous bow, was also brought forward in the Inui Laboratory of the Tokyo University (see Miyata et al. (1980, 1981, 1982)), and has been applied to the actual ship. The experimental results show an improved performance for such modified hull form.

Potential Theory of the Steady Ship Wave Problem

A moving Cartesian coordinate system is adopted as shown in Fig. 1, where oxyz moves steadily with the ship at speed U in the negative ox direction, and oxy coincides with the undisturbed waterplane. Under the assumption of potential flow and linearized free-surface boundary condition, the velocity potential $\Phi(x,y,z)$ of a fluid domain V surrounding the ship can be written as

$$\Phi(x,y,z) = Ux + \varphi(x,y,z) \qquad (1)$$

Here $\varphi(x,y,z)$ is the perturbation potential which perturbs the known basic flow potential Ux, and is the solution ot the boundary value problem consisting of:

the Laplace equation,

$$\nabla^2 \varphi(x,y,z) = 0, \qquad (2)$$

the linearized free-surface condition,

$$\frac{\partial^2 \varphi}{\partial x^2} + K_0 \frac{\partial \varphi}{\partial z} = 0, \qquad K_0 = g/U^2 \quad \text{on } z = 0 \qquad (3)$$

the hull-surface condition,

$$\frac{\partial \varphi}{\partial n} = -U\vec{n} \cdot \vec{i}, \qquad \text{on S} \qquad (4)$$

and the radiation condition,

$$\lim_{R\to\infty} \varphi = \begin{cases} o(1/R) \\ O(1/R) \end{cases}, \qquad R = \sqrt{x^2+y^2} \qquad (5)$$

where S is the wetted ship hull surface,

and $\vec{n}$ is the normal vector of S directed torward the

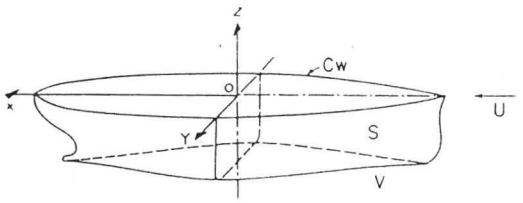

Fig. 1 Coordinate System

fluid domain V. The boundary value problem given by equations (2), (3), (4) and (5) is the well-known Neumann-Kelvin problem. In this problem the free-surface boundary condition is linearized whereas the hull-surface boundary condition is satisfied exactly. Introducing a Green's function $G(x,y,z;\xi,\eta,\zeta)$ known as the Havelock source function, and applying the Green's second identity, the perturbation potential $\varphi(x,y,z)$ satisfying equations (2), (3) and (5) can be represented by the following integral form [see, e.g., Liao (1973)],

$$\varphi(x,y,z) = \iint_S \sigma(\xi,\eta,\zeta)\cdot G(x,y,z;\xi,\eta,\zeta)\, ds - \frac{1}{4\pi K_0} \oint_C \sigma(\xi,\eta,\zeta)\cdot H(x,y,z;\xi,\eta,0) \cdot \vec{n}(\xi,\eta,0)\cdot \vec{i}\, d\eta, \qquad (6)$$

where the Havelock source function has the form of

$$G(x,y,z;\xi,\eta,\zeta) = -\frac{1}{4\pi}\left[\frac{1}{\sqrt{(x-\xi)^2+(y-\eta)^2+(z-\zeta)^2}} - \frac{1}{\sqrt{(x-\xi)^2+(y-\eta)^2+(z+\zeta)^2}} - H(x,y,z;\xi,\eta,\zeta)\right], \qquad (7)$$

$$H(x,y,z;\ \xi,\ \eta,\ \zeta)=$$
$$-4K_0\int_0^{\pi/2} d\theta\ \sec^2\theta \cdot e^{K_0(z+\zeta)\sec^2\theta}$$
$$\sin[K_0(x-\xi)\sec\theta]\cdot\cos[K_0(y-\eta)\sin\theta\cdot\sec^2\theta]$$
$$+\ \mathrm{Re}\left\{\frac{2K_0}{\pi}\int_{-\pi/2}^{\pi/2} d\theta\sec^2\theta\int_0^{\infty}\frac{\exp[k(z+\zeta)+ik\widetilde{\omega}]}{k-K_0\sec^2\theta}\,dk\right\}, \tag{8}$$

and

$$\widetilde{\omega} = (x-\xi)\cos\theta + (y-\eta)\sin\theta .$$

Equation (6) defines the potential $\varphi(x,y,z)$ as being caused by an equivalent source distribution $\sigma(x,y,z)$ over the hull surface S and the waterline C . Since the potential (6) should also satisfy the hull-surface boundary condition (4), then the boundary value problem defined by equations (2) to (5) may be replaced by an integral equation for the unknown function $\sigma(Q)$ distributed over S and C . Numerical solution of such integral equation for the computation of ship wave resistance has been accomplished by the authors, Tsai, Lin and Liao (1983). In the present study, the wave resistance is obtained by another approach in which a correlation between the wave profile and the wave resistance is used instead of the integral equation mentioned above. From the integral form of the potential $\varphi(x,y,z)$, the linearized free-surface elevation f(x,y) is given by

$$f(x,y) = -\frac{U}{g}\frac{\partial\varphi}{\partial x}(x,y,0)$$
$$= \frac{U}{g}\left\{\iint_S ds\,\sigma(\xi,\eta,\zeta) - \frac{1}{K_0}\oint_C d\eta\,\sigma(\xi,\eta,0)\,n_x(\xi,\eta,0)\right\}\cdot$$
$$\left\{\frac{K_0^2}{\pi}\int_0^{\pi/2} d\theta\sec^3\theta\cdot e^{K_0\zeta\sec^2\theta}\cdot\cos[K_0(x-\xi)\sec\theta]\cdot\cos[K_0(y-\eta)\sin\theta\cdot\sec^2\theta]\right.$$
$$+\frac{K_0}{\pi^2}\int_0^{\pi/2} d\theta\sec\theta\int_0^{\infty} dk\cdot k e^{k}\cdot\left.\frac{\sin[k(x-\xi)\cos\theta]\cdot\cos[k(y-\eta)\sin\theta]}{k-K_0\sec^2\theta}\right\}. \tag{9}$$

The wave resistance Rw acting upon the ship can be derived from the momentum consideration of fluid domain V, and represented by the so called amplitude functions $P(\theta)$ and $Q(\theta)$,

$$Rw = 16\rho\pi K_0^2\int_0^{\pi/2}[P(\theta)^2 + Q(\theta)^2]\sec^3\theta\,d\theta, \tag{10}$$

where

$$P(\theta)+iQ(\theta) =$$
$$\frac{1}{4\pi}\iint_S\sigma(\xi,\eta,\zeta)\exp\{K_0[\zeta+i(\xi\cos\theta+\eta\sin\theta)]\sec^2\theta\}\,ds$$
$$-\frac{1}{4\pi K_0}\oint_C\sigma(\xi,\eta,0)\exp\{iK_0(\xi\cos\theta+\eta\sin\theta)\sec^2\theta\}\cdot n_x(\xi,\eta,0)\,d\eta . \tag{11}$$

In the following discussions a relationship between the wave elevation and the ampljtude functions given by equations (9) and (11) is sought.

Correlation between Longitudinal Wave Profile and Wave Resistance

An expression for the amplitude functions $P(\theta)$ and $Q(\theta)$ in terms of the Fourier transform of the wave profile along the longtudinal cut is to be derived here. Taking the Fourier transform of f(x,y) with respect to x, and assuming that the order of the integration can be interchanged, one has

$$\int_{-\infty}^{\infty} f(x,y)e^{i\lambda x}\,dx = \lim_{M\to\infty}\int_{-M}^{M} f(x,y)\,e^{i\lambda x}\,dx$$
$$= \lim_{M\to\infty}\frac{U}{g}\left\{\iint_S ds\,\sigma(\xi,\eta,\zeta) - \frac{1}{K_0}\oint_C d\eta\,\sigma(\xi,\eta,0)\cdot n_x(\xi,\eta,0)\right\}\cdot$$
$$\left\{\frac{K_0^2}{\pi}\int_0^{\pi/2} d\theta\sec^3\theta\cdot e^{K_0\zeta\sec^2\theta}\cdot\cos[K_0(y-\eta)\sin\theta\cdot\sec^2\theta]\cdot\right.$$
$$\left.\sec^2\theta\cdot\int_{-M}^{M} dx e^{i\lambda x}\cos[K_0(x-\xi)\sec\theta]\right.$$
$$+\frac{K_0}{\pi^2}\int_0^{\pi/2} d\theta\int_0^{\infty} dk e^{k\zeta}\frac{k\cos\theta\cdot\cos[k(y-\eta)\sin\theta]}{k\cos^2\theta - K_0}$$
$$\left.\int_{-M}^{M} dx e^{i\lambda x}\sin[k(x-\xi)\cos\theta]\right\}$$
$$= \lim_{M\to\infty}\frac{U}{g}\left\{\iint_S ds\,\sigma(\xi,\eta,\zeta) - \frac{1}{K_0}\oint_C d\eta\,\sigma(\xi,\eta,0)\cdot n_x(\xi,\eta,0)\right\}\cdot$$
$$\left\{\frac{K_0^2}{\pi}\int_0^{\pi/2} d\theta\sec^3\theta\cdot e^{K_0\zeta\sec^2\theta}\cdot\cos[K_0(y-\eta)\sin\theta\cdot\sec^2\theta]\cdot\right.$$
$$\left.\left[\frac{\sin[(\lambda-K_0\sec\theta)M]}{\lambda-K_0\sec\theta} + \frac{\sin[(\lambda+K_0\sec\theta)M]}{\lambda+K_0\sec\right.\right.$$

$$\cdot \cos(K_o \xi \sec\theta) + i\left[\frac{\sin[(\lambda - K_o \sec\theta)M]}{\lambda - K_o \sec\theta} - \frac{\sin[(\lambda + K_o \sec\theta)M]}{\lambda + K_o \sec\theta}\right] \cdot \sin(K_o \xi \sec\theta) \}$$

$$+ \frac{K_o}{\pi^2} \int_0^{\pi/2} d\theta \int_0^{\infty} dk e^{k\zeta} \frac{k\cos\theta \cdot \cos[k(y-\eta)\sin\theta]}{k\cos^2\theta - K_o} \cdot \cdot$$

$$\{ \left[\frac{\sin[(\lambda - k\cos\theta)M]}{\lambda - k\cos\theta} - \frac{\sin[(\lambda + k\cos\theta)M]}{\lambda + k\cos\theta}\right]$$

$$\cdot \sin(k\xi\cos\theta) + i\left[\frac{\sin[(\lambda - k\cos\theta)M]}{\lambda - k\cos\theta} - \frac{\sin[(\lambda + k\cos\theta)M]}{\lambda + k\cos\theta}\right] \cdot \cos(k\xi\cos\theta) \} \}$$

$$\equiv \lim_{M\to\infty} \frac{U}{g} \{ \iint_S ds\,\sigma(\xi,\eta,\zeta) - \frac{1}{K_o} \oint_C d\eta\,\sigma(\xi,\eta,0) \cdot n_x(\xi,\eta,0) \} \cdot \{ \frac{K_o^2}{\pi} J_1 - \frac{K_o}{\pi^2} J_2 \}. \quad (12)$$

The integrals J_1 and J_2 in equation (12) can be evaluated by using the lemma described in Appendex A and by some derivations. Upon substitution of these results, equation (12) becomes

$$\int_{-\infty}^{\infty} f(x,y) e^{i\lambda x} dx$$

$$= \lim_{M\to\infty} \frac{U}{g} \{ \iint_S ds\,\sigma(\xi,\eta,\zeta) - \frac{1}{K_o} \oint_C d\eta\,\sigma(\xi,\eta,0)\, n_x(\xi,\eta,0) \} \cdot$$

$$\{ \frac{\lambda^2}{K_o} \exp[K_o \zeta (\lambda/K_o)^2] \cdot \frac{\cos[\lambda(y-\eta)\sqrt{(\lambda/K_o)^2 - 1}]}{\sqrt{(\lambda/K_o)^2 - 1}} \cdot e^{i\lambda\xi} \quad (13)$$

$$- i\frac{K_o}{\pi} e^{i\lambda\xi} \int_0^{\pi/2} d\theta\, e^{\frac{\lambda}{\cos\theta}\zeta} \cdot \frac{\lambda\cos[\lambda(y-\eta)\tan\theta]}{(\lambda - K_o\sec\theta)\cos^2\theta} \},$$

where λ must satisfies the condition $\lambda = K_o \sec\theta$. The principal value integral with respect to θ in equation (13) can further be evaluated by a suitable complex contour integration. By changing the integral variable θ with $t = \tan\theta$, and executing the contour integral along the contour in complex t plane as shown in Fig. 2, where $t_o = \sqrt{(\lambda/K_o)^2 - 1}$ is the pole, the following result can be obtained (see Appendix B),

$$\int_0^{\pi/2} d\theta\, e^{\frac{\lambda}{\cos\theta}\zeta} \cdot \frac{\lambda\cos[\lambda(y-\eta)\tan\theta]}{(\lambda - K_o\sec\theta)\cos^2\theta}$$

$$= \pi \left(\frac{\lambda}{K_o}\right)^2 \cdot \exp[K_o\zeta(\lambda/K_o)^2] \cdot \frac{\sin[\lambda(y-\eta)\sqrt{(\lambda/K_o)^2 - 1}]}{\sqrt{(\lambda/K_o)^2 - 1}} \cdot \quad (14)$$

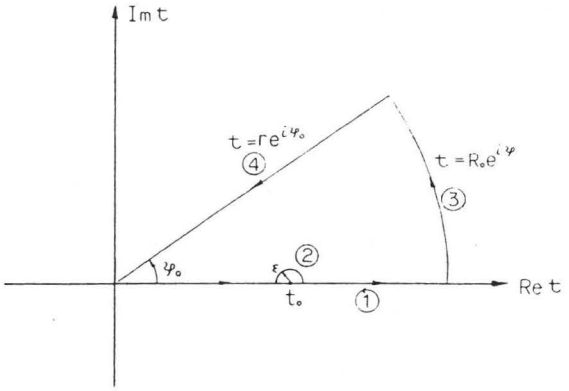

Fig. 2 Path of Contour Integral in Equation (13)

Substituting equation (14) into (13), one gets

$$\int_{-\infty}^{\infty} f(x,y) e^{i x K_o \sec\theta} dx$$

$$= \frac{g}{U} \{ \iint_S ds\,\sigma(\xi,\eta,\zeta) - \frac{1}{K_o} \oint_C d\eta\,\sigma(\xi,\eta,0)\, n_x(\xi,\eta,0) \} \cdot$$

$$\{ \frac{1}{K_o} \frac{\lambda^2}{\sqrt{(\lambda/K_o)^2 - 1}} \cdot \exp[K_o\zeta(\lambda/K_o)^2 + i[\lambda\zeta - \lambda(y-\eta)\sqrt{(\lambda/K_o)^2 - 1}]] \}$$

$$= \frac{e^{-iK_o y \sec\theta\tan\theta}}{U \sin\theta \cdot \cos\theta} \cdot$$

$$\{ \iint_S \sigma(\xi,\eta,\zeta) \exp\{ K_o [\zeta + i(\xi\cos\theta + \eta\sin\theta)] \sec^2\theta \} ds$$

$$- \frac{1}{K_o} \oint_C \sigma(\xi,\eta,0) \exp\{ iK_o(\xi\cos\theta + \eta\sin\theta)\sec^2\theta \} \cdot n_x(\xi,\eta,0)\, d\eta \}. \quad (15)$$

By comparing equation (15) with equation (11), the amplitude function $P(\theta)$, $Q(\theta)$ can be consequently expressed in the following form,

$$P(\theta) + iQ(\theta) = \frac{U}{4\pi} \sin\theta \cdot \cos\theta \cdot \exp(iK_o y \cdot \sec\theta \cdot \tan\theta) \cdot \int_{-\infty}^{\infty} f(x,y)\, e^{iK_o x \sec\theta} dx. \quad (16)$$

Similarly, by taking the Fourier transform of the longitudinal wave slope $f_x(x,y)$ and the transverse wave slope $f_y(x,y)$ along a longitudinal cut and following the foregoing procedures, the following two alternative expressions of the amplitude functions $P(\theta)$ and $Q(\theta)$ can also be obtained,

$$P(\theta)+iQ(\theta) = -\frac{U}{4\pi} i \sin\theta \cdot \cos^2\theta \cdot \exp(iK_0 y \cdot \sec\theta \cdot \tan\theta) \int_{-\infty}^{\infty} f_x(x,y) e^{iK_0 x \sec\theta} dx, \quad (17)$$

and

$$P(\theta)+iQ(\theta) = -\frac{U}{4\pi} i \cos^3\theta \cdot \exp(iK_0 y \sec\theta \cdot \tan\theta) \cdot \int_{-\infty}^{\infty} f_y(x,y) e^{iK_0 x \sec\theta} dx. \quad (18)$$

From equations (16), (17) and (18), it is found that if the wave elevation f, the longitudinal wave slope f_x or the transverse wave slope f_y can be measured along a longitudinal cut, i.e., along $y = y_0 =$ constant, then the wave resistance Rw can be obtained by use of equation (10).

In the present experimental work, only the equation (16) is used, that is only the longitudinal wave profile are measured for the wave resistance computations. For the convenience of numerical calculation equation (16) can further be rewritten in the following form,

$$\left.\begin{matrix} P(\theta) \\ Q(\theta) \end{matrix}\right\} = \frac{U}{4\pi} \sin\theta \cdot \cos\theta \left\{ \begin{matrix} \cos \\ \sin \end{matrix} (K_0 y_0 \tan\theta \cdot \sec\theta) \right.$$
$$\int_{-\infty}^{\infty} f(x,y_0) \cos(K_0 x \sec\theta)\, dx$$
$$\pm \begin{matrix} \sin \\ \cos \end{matrix} (K_0 y_0 \tan\theta \cdot \sec\theta) \int_{-\infty}^{\infty} f(x,y_0) \sin(K_0 x \sec\theta)\, dx \Big\}. \quad (19)$$

Truncation Correction

According to equation (19), the wave profile should be recorded from $-\infty$ to ∞ to complete the integration of this formula exactly. There are no wave in front of the ship, so that truncation of the wave record at some suitable position before the ship does not arise any problems. But for the wave profile behind the ship, due to the finite width of the towing tank, the wave reflected by the side walls of the tank will disturb the wave profile along the measurement track. On account of such facts, only a finite range of longitudinal wave profile is available for the actual calculation of the integral formula.

Fig. 3 is the illustration of the effect of reflective wave caused by the tank wall, where x = M is the point of truncation. An asymptotic approximation of the wave profile is taken to make up the truncated wave record, and to carry out the integration formula (19) from $-\infty$ to ∞. It is known that the wave profile far downstream has the following asymptotic behavior,

$$f(x,y) = f_0 \frac{\cos(K_0 + \varepsilon)}{\sqrt{K_0 x}} \qquad (x > M) \quad (20)$$

Here f_0 and ε are the constants which can be determined from the measured wave record by applying the least square method to some region before the truncation point. The detailed processes are described in Appendix C.

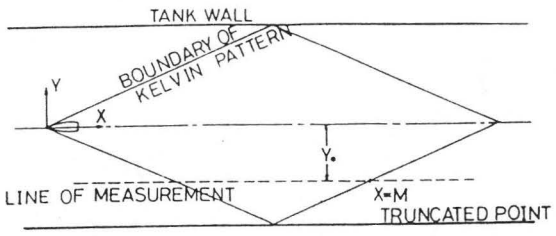

Fig. 3 Illustration of the Effect of Wave Reflection of the Side Walls

As the wave profile is given by a truncated measurement supplemented with the downstream approximation (20), equation (19) yields the amplitude functions in the following form,

$$\left.\begin{matrix} P(\theta) \\ Q(\theta) \end{matrix}\right\} = \frac{U}{4\pi} \sin\theta \cdot \cos\theta \cdot \left\{ \begin{matrix} \cos \\ \sin \end{matrix} (K_0 y_0 \tan\theta \cdot \sec\theta) \cdot \right.$$
$$\Big[\int_{-\infty}^{M} f(x,y_0) \cdot \cos(K_0 x \sec\theta) dx +$$
$$\int_{M}^{\infty} f_0 \frac{\cos(K_0 x + \varepsilon)}{\sqrt{K_0 x}} \sin(K_0 x \sec\theta)\, dx \Big]$$
$$\pm \begin{matrix} \sin \\ \cos \end{matrix} (K_0 y_0 \tan\theta \cdot \sec\theta) \cdot$$
$$\Big[\int_{-\infty}^{M} f(x,y_0) \cdot \sin(K_0 x \sec\theta)\, dx +$$
$$\int_{M}^{\infty} f_0 \frac{\cos(K_0 x + \varepsilon)}{\sqrt{K_0 x}} \cos(K_0 x \sec\theta) dx \Big] \Big\}. \quad (21)$$

The integral terms $\int_M^\infty f_0 \frac{\cos(K_0x + \varepsilon)}{\sqrt{K_0x}} \begin{matrix}\sin\\ \cos\end{matrix}(K_0x\sec\theta)dx$ in the above equation can further be expressed as (see Appendix D)

$$\int_M^\infty f_0 \frac{\cos(K_0x + \varepsilon)}{\sqrt{K_0x}} \begin{matrix}\sin\\ \cos\end{matrix}(K_0x\sec\theta)dx$$

$$= \sqrt{\frac{\pi}{2}}\frac{f_0}{K_0}\left\{\frac{\cos\varepsilon}{\sqrt{\sec\theta+1}}\left[\frac{1}{2} - \int_0^{\sqrt{MK_0(\sec\theta+1)}\sqrt{\frac{2}{\pi}}} \begin{matrix}\cos\\ \sin\end{matrix}\left(\frac{\pi}{2}t^2\right)dt\right] + \right.$$

$$\frac{\cos\varepsilon}{\sqrt{\sec\theta-1}}\left[\frac{1}{2} - \int_0^{\sqrt{MK_0(\sec\theta-1)}\sqrt{\frac{2}{\pi}}} \begin{matrix}\cos\\ \sin\end{matrix}\left(\frac{\pi}{2}t^2\right)dt\right]$$

$$\mp\frac{\sin\varepsilon}{\sqrt{\sec\theta+1}}\left[\frac{1}{2} - \int_0^{\sqrt{MK_0(\sec\theta+1)}\sqrt{\frac{2}{\pi}}} \begin{matrix}\cos\\ \sin\end{matrix}\left(\frac{\pi}{2}t^2\right)dt\right]$$

$$\left.\pm\frac{\sin\varepsilon}{\sqrt{\sec\theta-1}}\left[\frac{1}{2} - \int_0^{\sqrt{MK_0(\sec\theta-1)}\sqrt{\frac{2}{\pi}}} \begin{matrix}\cos\\ \sin\end{matrix}\left(\frac{\pi}{2}t^2\right)dt\right]\right\}, \qquad (22)$$

where $\int_0^{\sqrt{z}\sqrt{\frac{2}{\pi}}} \begin{matrix}\sin\\ \cos\end{matrix}\left(\frac{\pi}{2}t^2\right)dt$ is the so called Fresnel's integrals. Equations (19), (21) and (22) are the formulas for the numerical computations of ship wave-resistance from longitudinal wave-height measurement. For convenience, the wave resistance is expressed in the nondimensional form,

$$C_W = \frac{R_W}{\frac{1}{2}\rho U^2L^2} = 2\pi\int_0^{\pi/2} A^*(\theta)^2 d\theta$$

$$= 2\pi\int_0^{\pi/2} [C^*(\theta)^2 + S^*(\theta)^2]d\theta, \qquad (23)$$

where $\left.\begin{matrix}C^*(\theta)\\ S^*(\theta)\end{matrix}\right\} = \frac{4K_0}{UL}\sec^{3/2}\theta\left\{\begin{matrix}P(\theta)\\ Q(\theta)\end{matrix}\right.$ are called the weighted amplitude functions.

On-Line Experimental System

To make the experiment and analysis automatic, a microcomputer is applied to control the measuring procedure, and to execute the data management and computation. Fig. 4 shows the total equipments of the experimental system.

The experiment was carried out in the model basin of the Institute of Naval Architecture, the National Taiwan University. The towing tank is 150m long with a 4 m wide by 2 m deep rectangular

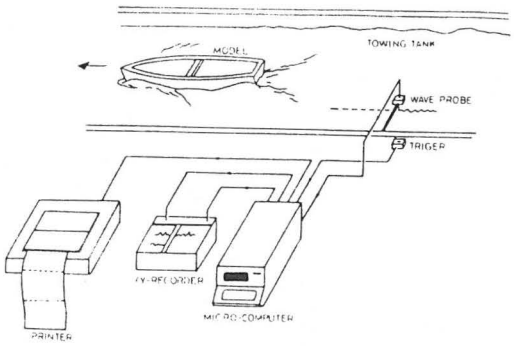

Fig. 4 Equipments of the On-Line Wave Analysis Experimental System

section. The microcomputer has several special functions, such as discrete analog-signal input and output, and averaging of the discrete input data, etc.. The wave height probe is of the capacitance type, mounted at a distance off the tank centerline by a fixed arm as shown in Fig. 5. A switch setted on the side of the tank rail and an electric circuit connected with the microcomputer form a trigger. The trigger circuit will be cut down by the towing carriage when a chosen point of the carriage passes the wave probe. The point is chosen to be at a suitable distance from the front of the bow wave. The microcomputer begins to input the wave height signal in voltage from the wave probe in a discrete rate as soon as the trigger circuit is cut down. The peripheral devices of the microcomputer include a X-Y recorder and a printer, used to plot the recorded wave profiles and print the computational results.

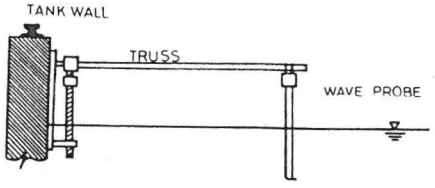

Fig. 5 Arrangement of the Wave Probe

The program of the microcomputer is written in the interactive BASIC language. Fig. 6 is the block diagram of the experimental procedure, which is also

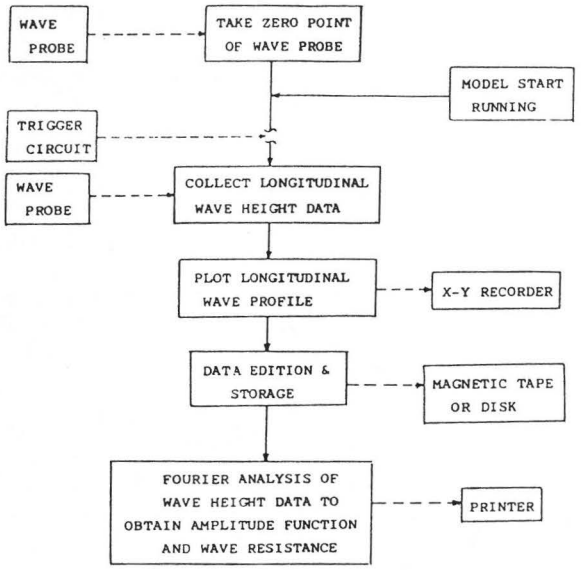

Fig. 6 Block Diagram of the Procedure of Wave Analysis Experiment

the flow chart of the control and computation program of the microcomputer. Operation of the entire experiment is described as follows:

1) The zero point of the wave probe is determined before the carriage running by recording the voltage signal of the calm free-surface and taking the average of the value. Then the carriage with the model starts running.

2) The cut down of the trigger circuit, and the input of the wave height records from the wave probe are continuously and simultaneously done. The recording rate is 100 signal/sec in the present experiment. The recorded data is stored in the core memory of the microcomputer temporarily.

3) The wave profile is plotted by the X-Y recorder. The point where reflective wave begins to affect can be approximately calculated from the geometry in Fig. 3. By these two kinds of information the point of truncation can be determined.

4) The wave height data which is provided for the computation of wave resistance is edited and stored in the magnetic tape of the microcomputer.

5) Numerical analysis of the recorded data by the foregoing formulas is carried out to compute the wave resistance. The information output from the printer includes the identifications of the experiment (such as model name, Froude number, probe calibrating value, etc.), the discrete wave height data, the constants f_0 and ε for the truncation correction, the weighted amplitude functions $C^*(\theta)$, $S^*(\theta)$ and $A^*(\theta)$, and the wave resistance coefficient Cw.

The procedures described above is executed per running of the model, and the edition and analysis of the data can be proceeded when the carriage is waiting for the stillness of the free surface in the basin.

Experimental Results

A. Parabolic Hull Form

To verify the validity of the experimental system, a simple hull form, the parabolic hull form is used for the test first. Fig. 7 is the body plan of the hull form, which is a simple wave-making mechanism. The equation of the hull surface is

$$y(x,z) = \frac{\bar{B}}{2}\left[1 - \left(\frac{2x}{L}\right)^2\right] \cdot \left[1 - \left(\frac{z}{D}\right)^2\right],$$

where $\bar{B}/L = 0.1$ and $D/L = 0.1$. The length of the model L is 3 m and its draft H is 0.225 m, that is $H/L = 0.075$ and $B/L = 0.09375$, where B is the beam at midship of the waterplane.

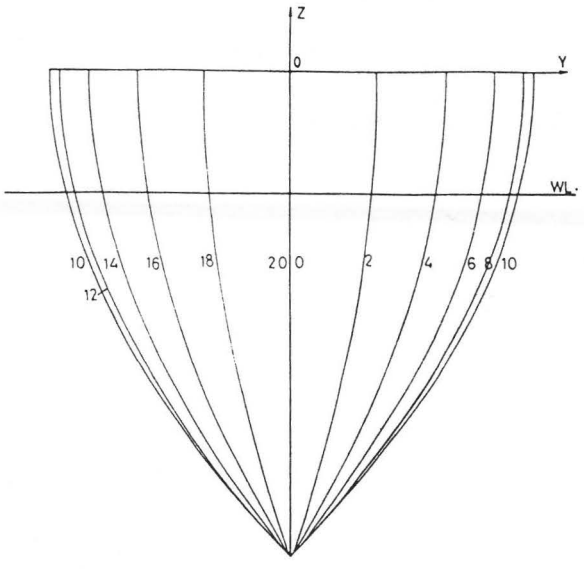

Fig. 7 Body Plan of the Parabolic Hull Form

The model is fixed to the carriage and not free to squat and trim when it runs. Experiments were run on the model at seven Froude numbers with two y_o variations for each case, where y_o is the distance laterally away from the centerline to the position of wave probe. The two positions of wave probe are y_o/L = 0.2 and y_o/L = 0.1. Results of wave analysis at two measured positions for the wave resistance of the parabolic hull form are listed in Table 1 and illustrated in Fig. 8, and the weighted amplitude function $A^*(\theta)$ are shown in Fig. 9 to Fig. 15 for each Froude number. It is found that the results of y_o/L = 0.2 are slightly larger than those of y_o/L = 0.1. The differences of results between these two measured positions are quite little, except the case of Fn =0.302 (K_oL = 11). One of the explanations for such phenomenon is the misjudgement of the truncation point. Fig. 16 to Fig. 22 are some portion of the wave profile recorded at two measured positions for each Froude number.

K_oL	Fn	$C_W \times 10^4$	
		Y_o/L=0.2	Y_o/L=0.1
14	0.267	1.0204	0.9766
13	0.278	1.2809	1.1190
12	0.288	1.5250	1.4271
11	0.302	1.9877	1.6762
10	0.317	1.9711	1.8537
9	0.344	1.7870	1.7474
8	0.356	1.6076	1.5204

Table 1 Results of Wave Analysis for the Parabolic Hull Form

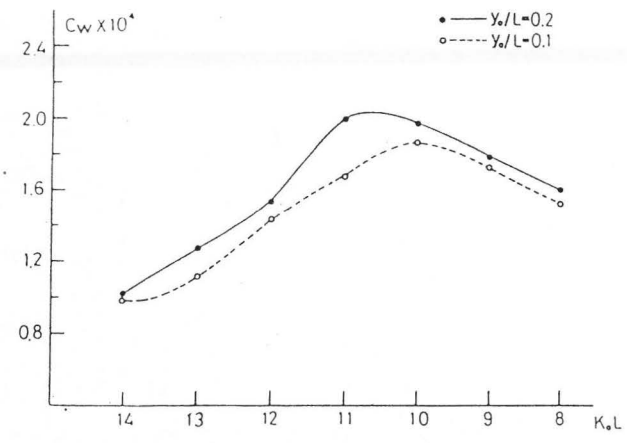

Fig. 8 Results of Wave Analysis for the Parabolic Hull Form

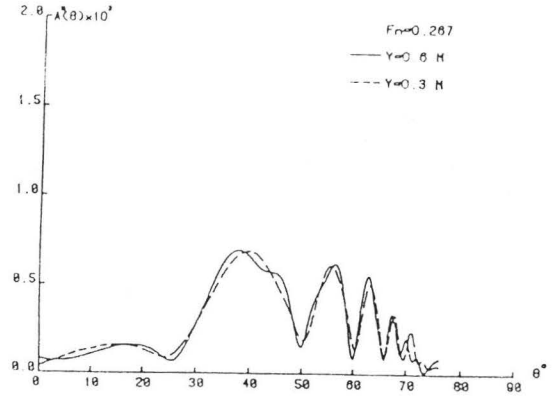

Fig. 9 Amplitude Functions of the Parabolic Hull Form at KoL=14, Fn=0.267

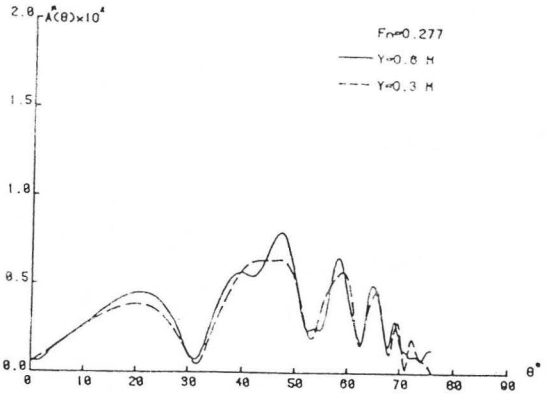

Fig. 10 Amplitude Functions of the Parabolic Hull Form at KoL=13, Fn=0.277

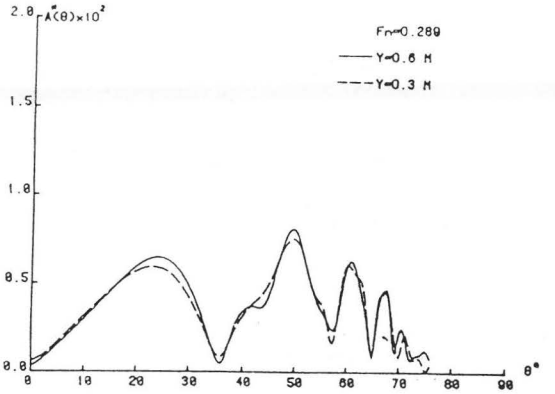

Fig. 11 Amplitude Functions of the Parabolic Hull Form at KoL=12, Fn=0.289

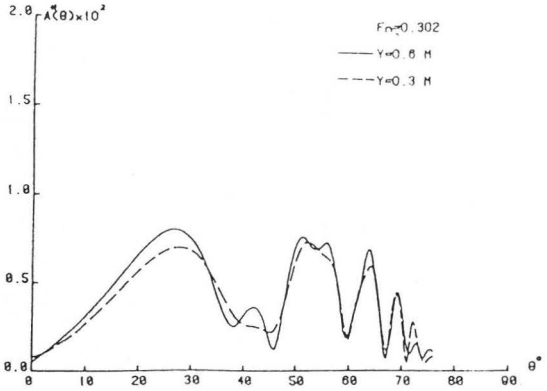

Fig. 12 Amplitude Functions of the Parabolic Hull Form at KoL=11, Fn=0.302

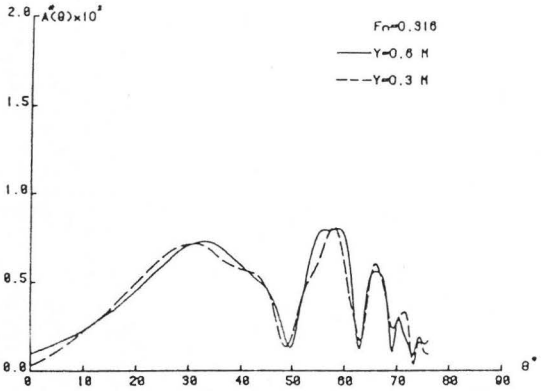

Fig. 13 Amplitude Functions of the Parabolic Hull Form at KoL=10, Fn=0.316

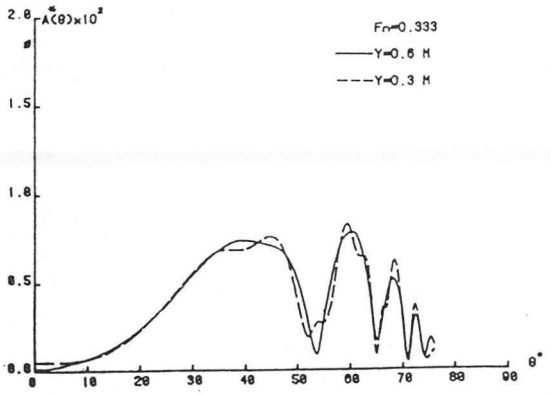

Fig. 14 Amplitude Functions of the Parabolic Hull Form at KoL=9, Fn=0.333

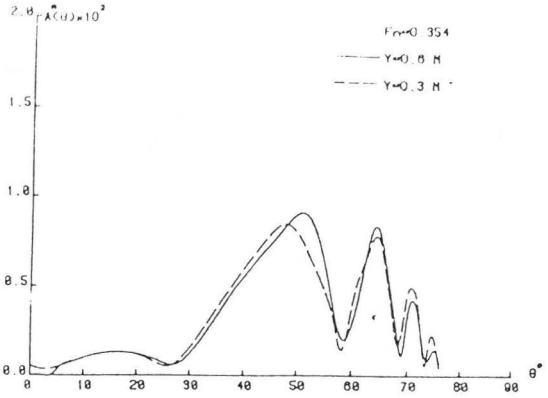

Fig. 15 Amplitude Functions of the Parabolic Hull Form at KoL=8, Fn=0.354

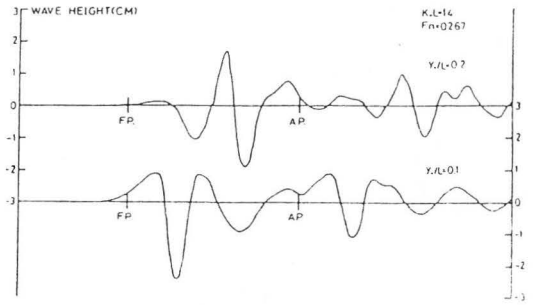

Fig. 16 Longitudinal Wave Profiles of the Parabolic Hull Form at KoL=14, Fn=0.267

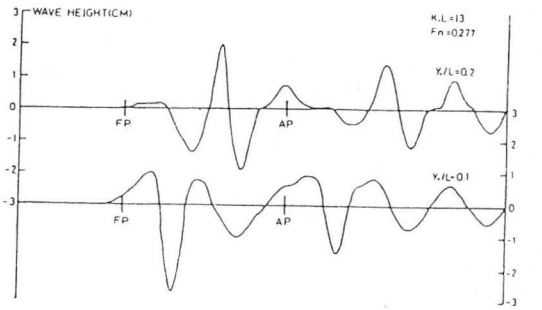

Fig. 17 Longitudinal Wave Profiles of the Parabolic Hull Form at KoL=13, Fn=0.277

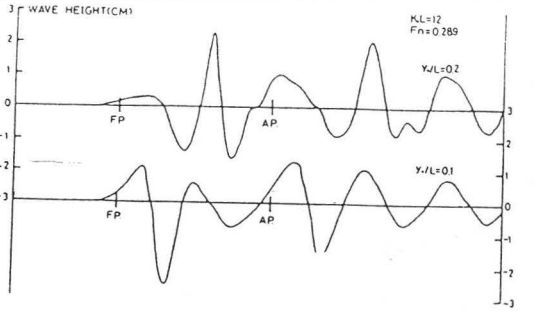

Fig. 18 Longitudinal Wave Profiles of the Parabolic Hull Form at KoL=12, Fn=0.289

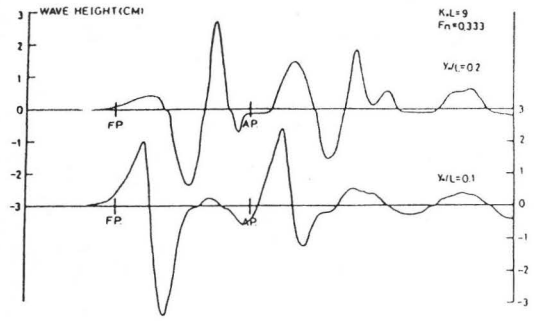

Fig. 19 Longitudinal Wave Profiles of the Parabolic Hull Form at KoL=11, Fn=0.302

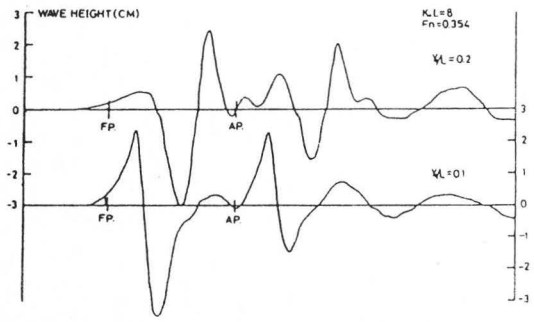

Fig. 20 Longitudinal Wave Profiles of the Parabolic Hull Form at KoL=10, Fn=0.316

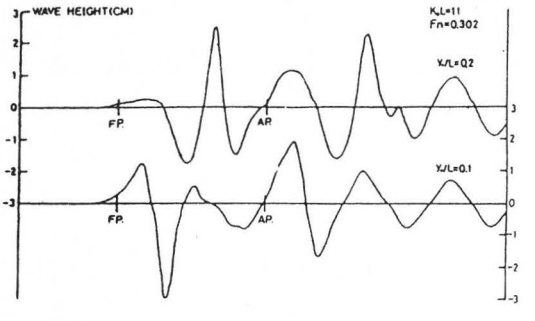

Fig. 21 Longitudinal Wave Profiles of the Parabolic Hull Form at KoL=9, Fn=0.333

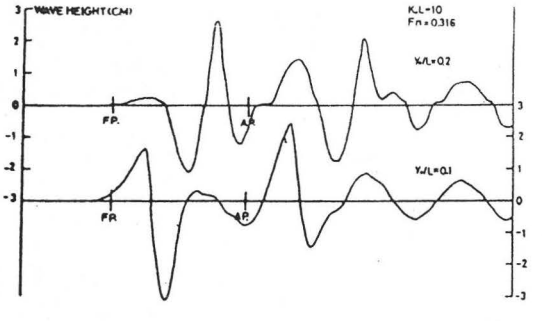

Fig. 22 Longitudinal Wave Profiles of the Parabolic Hull Form at KoL=8, Fn=0.354

B. Destroyer Hull Form

Fig. 23 is the body plan of the destroyer hull form. Its model number is MS017 and with the principal particulars as follows,

Lpp = 232.76 cm,

B = 26.94 cm,

H = 8.20 cm.

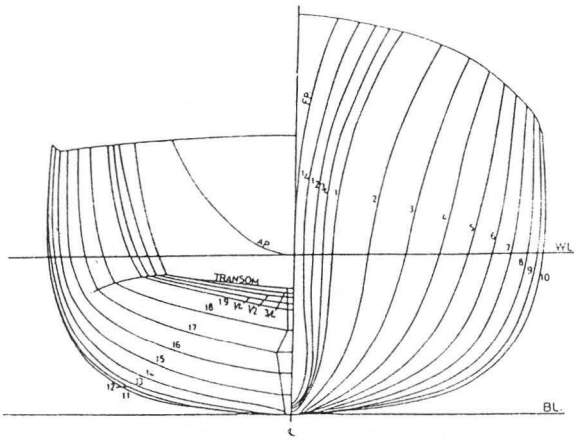

Fig. 23 Body Plan of the Destroyer Hull Form MS017

Both resistance test and wave pattern analysis were performed simultaneously. With the towing arrangements being used, the model was permitted to seek its equilibrium trim and sinkage. The position of the wave probe is at y_o = 46.6cm, i.e., y_o = 0.2 Lpp.

A bulbous bow and a stern-end-bulb, made from wax, were attached to the parent model MS017 and named MS017D. Fig. 24 is the configuration of the bulbous bow and stern-end-bulb. Resistance test and wave pattern analysis were also implemented for the improved hull form MS017D.

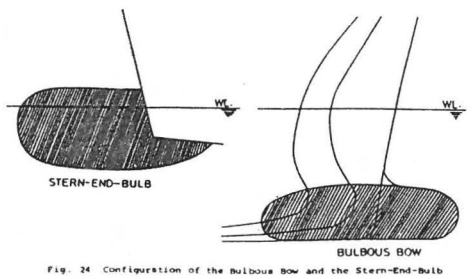

Fig. 24 Configuration of the Bulbous Bow and the Stern-End-Bulb

Table 2 shows the results of resistance test and wave analysis. The total resistance coefficients for both MS017 and MS017D are shown in Fig. 25, and the wave resistance coefficients obtained from resistance test and wave pattern analysis for both two models are illustrated in Fig. 26. The amplitude functions and longitudinal wave profiles obtained from wave pattern analysis are shown in Fig. 27 to Fig. 31 and Fig. 32 to Fig. 36 respectively. From above experimental results, it is seen that the improved hull form MS017D achieves a reduction of total resistance and wave resistance.

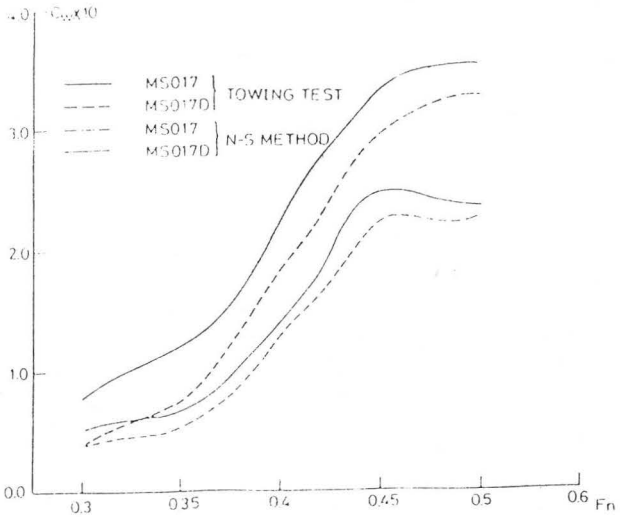

Fig. 26 Wave-Resistance Coefficients of MS017 and MS017D from Resistance Test and Wave Analysis

Fn	Ct x 10^4		Cw x 10^4 Towing Test		Cw x 10^4 Wave Analysis	
	MS017	MS017D	MS017 K=0.12	MS017D K=0.08	MS017	MS017D
0.225	5.262	5.168	0.328	0.047	0.185	0.142
0.250	5.339	5.119	0.496	0.095	0.301	0.164
0.275	5.367	5.127	0.613	0.184	0.392	0.213
0.300	5.467	5.274	0.771	0.401	0.496	0.386
0.325	5.633	5.388	1.006	0.580	0.594	0.456
0.350	5.776	5.469	1.211	0.727	0.671	0.511
0.375	6.098	5.892	1.586	1.203	0.995	0.786
0.400	6.733	6.460	2.269	1.825	1.441	1.300
0.425	7.234	7.035	2.811	2.451	1.864	1.744
0.450	7.653	7.480	3.275	2.935	2.470	2.249
0.475	7.831	7.684	3.494	3.180	2.413	2.230
0.500	7.839	7.740	3.537	3.266	2.373	2.261

Table 2 Results of Towing Test and Wave Analysis for MS017 and MS017D

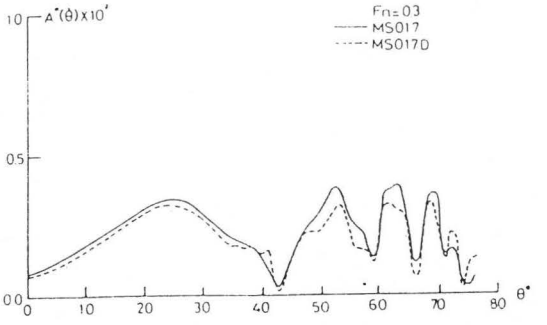

Fig. 27 Amplitude Functions of MS017 and MS017D at Fn=0.3

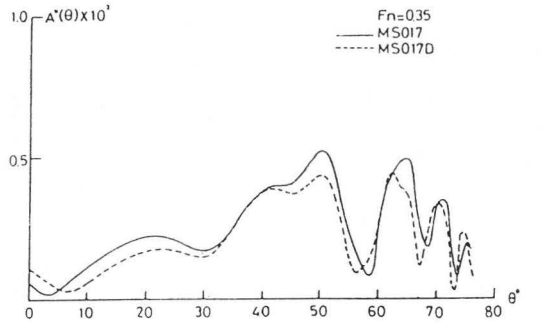

Fig. 28 Amplitude Functions of MS017 and MS017D at Fn=0.35

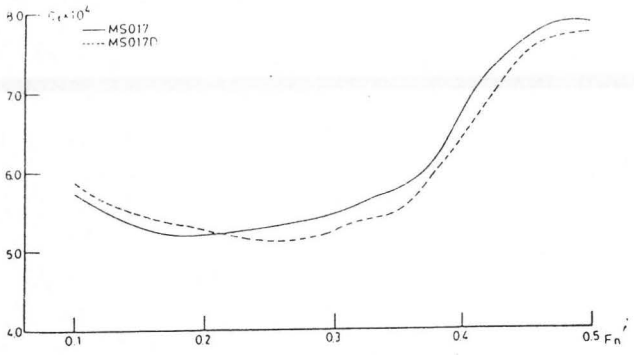

Fig. 25 Resistance Test Results of MS017 and MS017D

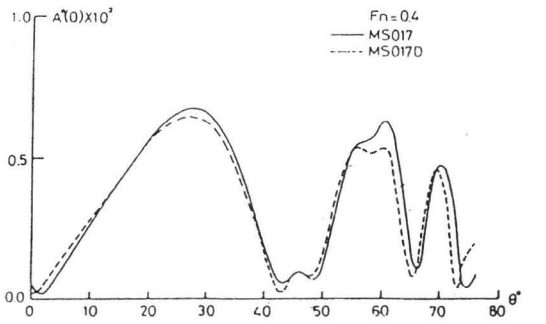

Fig. 29 Amplitude Functions of MS017 and MS017D at Fn=0.4

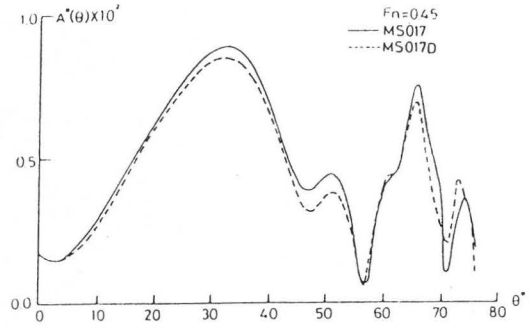

Fig. 30 Amplitude Functions of MS017 and MS017D at Fn=0.45

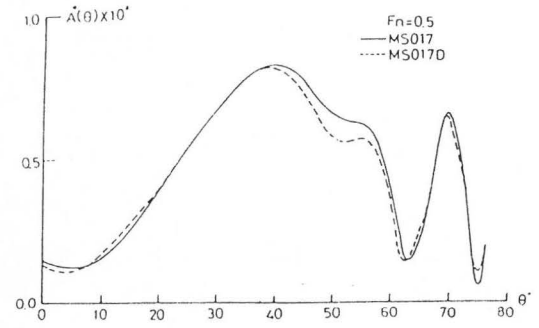

Fig. 31 Amplitude Functions of MS017 and MS017D at Fn=0.5

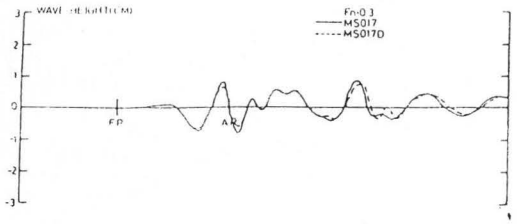

Fig. 32 Longitudinal Wave Profiles of MS017 and MS017D at Fn=0.3

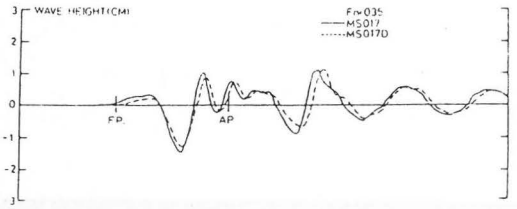

Fig. 33 Longitudinal Wave Profiles of MS017 and MS017D at Fn=0.35

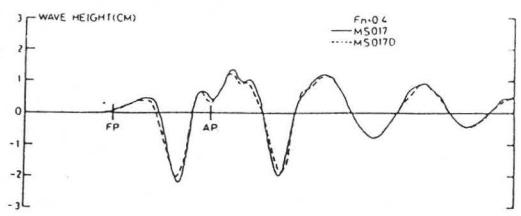

Fig. 34 Longitudinal Wave Profiles of MS017 and MS017D at Fn=0.4

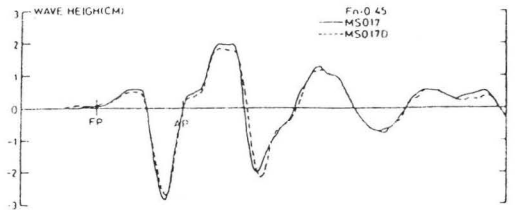

Fig. 35 Longitudinal Wave Profiles of MS017 and MS017D at Fn=0.45

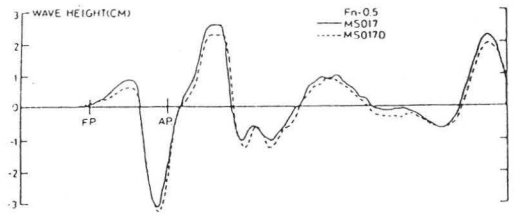

Fig. 36 Longitudinal Wave Profiles of MS017 and MS017D at Fn=0.5

Conclusions and Recomendatons

Longitudinal wave-pattern analysis method was accomplished for the direct determination of ship wave resistance. The online experimental system was established in the towing tank of the Institute of Naval Architecture, the National Taiwan University. The wave analysis experiments were carried out for a parabolic hull form and for a destroyer hull form. Based upon the preceding results of experiments, the following conclusions are drawn and recomendations are made:

1) The asymptotic wave-profile approximation (20) is valid near the centerline, while the formulations of longitudinal wave pattern analysis is derived under the condition $y \to \infty$, so that a further study should be made for such discrepancy and to find a reasonable position of measurement in a towing tank of finite width.

2) The wave analysis method proposed in the present study is based upon the potential theory of steady ship wave problem the free-surface boundary condition is linearized. In the authors' opinions, the error due to the nonlinearity of free-surface boundary conditions or local-wave components are of less importance than

the discrepancy described above provided that the free surface is not breaking.

3) It is noticeable that the modified destroyer hull form MS017D with a bulbous bow and a stern-end-bulb achieves a considerable reduction of resistance compared to its parent hull form MS017. Further arrangement of a systematic experiment or a theoretical analysis should then be desirable for studying the causes of such improvement.

Acknowledgemnts

The authors wish to express their sincere gratitude to the staff of towing tank of the Institute of Naval Architecture, the National Taiwan University for the assistance in establishing the experimental system and implementing the experiments.

Professor Wei-yuan Hwang is also gratefully acknowledged for reviewing the manuscript and giving useful comments.

References

1 Adachi, H., "On Some Experimental Results of a Ship with Extremely Long-Parallel Middle-Body," Report of Ship Research Institute, Vol. 10, No. 4, 1973. pp. 159-173, (in Japanese).

2 Eggers, K. W. H., Sharma, S. D. and Ward, L. W., "An Assessment of Some Experimental Methods for Determinating the Wavemaking Characteristics of a Ship Form," Trans. SNAME, Vol. 75, 1967, pp. 112-144.

3 Ikehata, M. and Nozawa, K., "Determination of Wave-Making Resistance of a Ship by the Method of Wave Analysis," J. Soc. Naval Arch. Japan, Vol. 121, 1967, pp. 65-74, (in Japanese).

4 Ikehata, M. and Nozawa, K., "Determination of Wave-Making Resistance of a Ship by the Method of Wave Analysis (2nd Report)," J. Soc. Naval Arch. Japan, Vol. 124, 1968, pp. 1-13, (in Japanese).

5 Inui, T., Kajitani, H., Narita, H. and Mori, K., "Wave Analysis of Simple Hull Forms-Effects of Frameline Forms (the Second Report)," J. Soc. Naval Arch. Japan, Vol. 128, 1970, pp. 11-18, (in Japanese).

6 Lee, C., "Correlation of Longitudinal Wave Profiles and the Wave Resistance of a Ship Model, with a Proposed Local-Disturbance Correction," Univ. Michigan, Dept. Naval Arch. and Marine Eng., Report No. 092, 1969, 135pp..

7 Liao, C. C., "On the Potential Theory Applied to the Steady Ship Wave Problem," Doctoral Thesis, Dept. Naval Arch., Univ. Tokyo, Dec. 1973, 133 pp..

8 Michelson, F. and Uberoi, S. B. S., "A Study of Wave Resistance Characteristics Through the Analysis of Wave height and Slope Along a Longitudinal Track." Hydro-og Aerodynamisk Laboratorium, Report No. Hy-15, 1971, 30 pp..

9 Miyata, H., Tsuchiya, Y., Inui, T. and Adachi, H., "Resistance Reduction by Stern-End-Bulb (First Report)," J. Soc. Naval Arch. Japan, Vol. 148, 1980, pp. 10-16.

10 Miyata, H., Yoshihiro, T. and Inui, T., "Resistance Reduction by Stern-End-Bulb (Second Report)," J. Soc. Naval Arch. Japan, Vol. 149, 1981, pp. 1-10.

11 Newman, J. N., "The Determination of Wave Resistance from Wave Measurements along a Parallel Cut," Proc. Int. Seminar on Theoretical Wave Resistance, Univ. Michigan, Ann Arbor, 1963, pp. 353-379.

12 Okamoto, H., Tanaka, A., Yamano, T., Inui, T. and Miyata, H. "Resistance Reduction by Stern-End-Bulb (Third Report)," J. Soc. Naval Arch. Japan, Vol. 152, 1982, pp. 22-31.

13 Pien, P. C. and Moore, W. L., "Theoretical and Experimental Study of Wave-Making Resistance of Ships," Proc. Int. Seminar on Theoretical Wave Resistance, Univ. Michigan, Ann Arbor, 1963, pp. 353-376.

14 Sharma, S. D., "A Comparison of the Calculated and Measured Free-Wave Spectrum of a Inuid in Steady Motion," Proc. Int. Seminar on Theoretical Wave Resistance, Univ. Michigan, Ann Arbor, 1963,

pp. 201-257.

15 Sharma, S. D., "An Attempted Applicated of Wave Analysis Techniques to Achieve Bow-Wave Reduction," Proc. Sixth Symposium on Naval Hydrodynamics, Washington D. C., 1966, pp. 731-773.

16 Shor, W. W., "A Fourier Transform Method for Calculating Wave Making Resistance from Wave Height on a Line Parallel to a Ship Track," Proc. Int. Seminar on Theoretical Wave Resistance, Univ. Michigan, Ann Arbor, 1963, pp. 601-615.

17 Tsai, C. E. and Landweber, L., "Further Development of a Procedure for Determination of Wave Resistance from Longitudinal-Cut Surface-Profile Measurement," J. Ship Res., Vol. 19, No. 2, 1975, pp. 65-75.

18 Tsai, W. T., Lin, Y. J. and Liao, C. C., "Numerical Solution of the Neumann-Kelvin Problem and Its Application to Ship Wave-Resistance Computations," to be published.

19 Ward, L. W. and van Hooff, R. W., "The Effect of probe Location on a Model Wave Resistance Survey along a Longitudinal Cut," J. Ship Res., Vol. 20, No. 1, 1976, pp. 7-21.

Appendix A Evaluation of $\lim_{M\to\infty} J_{1,2}$ in Equation (12)

$\lim_{M\to\infty} J_{1,2}$ can be evaluated if the following lemma is used,

$$\begin{cases} \lim_{t\to\infty} \int_a^b F(k)\,\frac{\sin[tg(k)]}{g(k)}\,dk = \begin{cases} \pi \frac{F(k_0)}{|g'(k_0)|}, & (a<k_0<b) \\ 0, & (k_0<a \text{ or } k_0>b) \end{cases} \\ \lim_{t\to 0} \int_a^b F(k)\,\frac{\cos[tg(k)]}{g(k)}\,dk = 0, \end{cases}$$

where k_0 is the root of the equation $g(x) = 0$, and $g'(k_0) \neq 0$.

Let consider $\lim_{M\to\infty} J_1$ first, which is

$$\lim_{M\to\infty} J_1 = \lim_{M\to\infty} \int_0^{\infty} d\theta \sec^3\theta \cdot e^{K_0 \zeta \sec^2\theta} \cdot \cos[K_0(y-\eta)\sin\theta \cdot \sec^2\theta]$$

$$\left\{ \left[\frac{\sin[(\lambda - K_0\sec\theta)M]}{\lambda - K_0\sec\theta} + \frac{\sin[(\lambda + K_0\sec\theta)M]}{\lambda + K_0\sec\theta} \right] \cdot \cos(K_0 \xi \sec\theta) + i \left[\frac{\sin[(\lambda - K_0\sec\theta)M]}{\lambda - K_0\sec\theta} - \frac{\sin[(\lambda + K_0\sec\theta)M]}{\lambda + K_0\sec\theta} \right] \cdot \sin(K_0 \xi \sec\theta) \right\}.$$

Let $g_1(\theta) = \lambda - K_0\sec\theta$, $g_2(\theta) = \lambda + K_0\sec\theta$, and $g_1(\theta_1) = \lambda - K_0\sec\theta_1 \equiv 0$, $g_2(\theta_2) = \lambda + K_0\sec\theta_2 \equiv 0$.

It can be easily shown that the root of $g_2(\theta_2) = 0$ is not in the interval of integration, so that from the lemma the integrands whose denominator is $\lambda + K_0\sec\theta$ make no contribution to the integral. The root of $g_1(\theta_1) = 0$ is

$$0 < \theta_1 = \cos^{-1}\frac{K_0}{\lambda} < \frac{\pi}{2},$$

and

$$|g_1'(\theta_1)| = K_0\sec\theta_1 \cdot \tan\theta_1 = \lambda\sqrt{\left(\frac{\lambda}{K_0}\right)^2 - 1}.$$

It is of course necessary to satisfy the condition $\lambda \geq K_0 > 0$. Notice that λ has been assumed to be positive when the Fourier transform of f(x,y) is taken with respect to x. Then from the lemma, the results of $\lim_{M\to\infty} J_1$ is given by

$$\lim_{M\to\infty} J_1 = \pi \left(\frac{\lambda}{K_0}\right)^3 \cdot \exp\left[K_0 \zeta \left(\frac{\lambda}{K_0}\right)^2\right] \cdot \frac{\cos[\lambda(y-\eta)\sqrt{(\lambda/K_0)^2 - 1}]}{\lambda\sqrt{(\lambda/K_0)^2 - 1}} [\cos(\xi\lambda) + i\sin(\xi\lambda)],$$

where λ satisfies the condition $\lambda = K_0\sec\theta$.

Similarily, one can obtain

$$\lim_{M\to\infty} J_2 = \pi e^{\frac{\lambda}{\cos}\zeta} \cdot \frac{\lambda\cos[\lambda(y-\eta)\tan\theta]}{\lambda\cos\theta - K_0} \cdot \left[-\frac{\sin\lambda\xi}{\cos\theta} + i\frac{\cos\lambda\xi}{\cos\theta} \right],$$

where λ also satisfies $\lambda = K_0\sec\theta$.

Appendix B Evaluation of the Principal Value Integral wit Respect to θ in Equation (13)

Upon transformation of the integral variable θ with $t = \tan\theta$, the integral term with respect to θ in equation (13) becomes

$$\int_0^{\pi/2} d\theta\, e^{\frac{\lambda}{\cos\theta}\zeta} \cdot \frac{\lambda\cos[\lambda(y-\eta)\tan\theta]}{(\lambda - K_o\sec\theta)\cos^2\theta}$$

$$= \int_0^{\infty} dt\, e^{\lambda\zeta\sqrt{1+t^2}} \cdot \frac{\cos[\lambda(y-\eta)t]}{1 - \frac{K_o}{\lambda}\sqrt{1+t^2}}$$

$$= \mathrm{Re}\left\{\int_0^{\infty} dt \frac{\exp\{\lambda[\zeta\sqrt{1+t^2} + i(y-\eta)t]\}}{1 - \frac{K_o}{\lambda}\sqrt{1+t^2}}\right.$$

$$\equiv \mathrm{Re}\{\mathrm{P.V.}\int_0^{\infty} F(t)dt\}.$$

The principal value integral can be evaluated by taking the contour integral along the path as shown in Fig. 2, where $t_o = \sqrt{(\lambda/K_o)^2 - 1}$ is the pole. The contributions of the integral for each path are

path 1

$$\lim_{\varepsilon\to 0}\int_{①} F(t)dt = \mathrm{P.V.}\int_0^{\infty} F(t)dt,$$

path 2

$$\lim_{\varepsilon\to 0}\int_{②} F(t)dt = -\pi i \operatorname*{Res}_{t=t_o} F(t)$$

$$= \pi i \frac{(\lambda/K_o)^2}{\sqrt{(\lambda/K_o)^2 - 1}} \cdot$$

$$\exp\{\lambda[\zeta(\frac{\lambda}{K_o}) + i(y-\tau)\sqrt{(\frac{\lambda}{K_o})^2 - 1}]\},$$

path 3

$$\lim_{R_o\to\infty}\int_{③} F(t)dt = \lim_{R_o\to\infty}\int_{\infty}^{0} dr\, e^{i\varphi_o} \cdot$$

$$\frac{\exp\{\lambda[\zeta\sqrt{1+r^2e^{i2\varphi_o}} + i(y-\eta)re^{i\varphi_o}]}{1 - K_o/\lambda}$$

$$= \lim_{R_o\to\infty}\left\{\int_0^{\varphi_o} d\varphi\, ie^{i\varphi} \cdot R_o\exp\{\lambda\zeta\sqrt{1+R_o^2e^{2i\varphi}}\}\right.\cdot$$

$$\exp\{-\lambda(y-\tau)R_o\sin\varphi\} \cdot \frac{\exp\{i\lambda(y-\tau)R_o\cos\theta\}}{1 - \frac{K_o}{\lambda}\sqrt{1 + R_o^2e^{i2\varphi}}}$$

$$\to 0$$

path 4

$$\lim_{R_o\to\infty}\int_{④} F(t)dt = \int_{\infty}^{0} dr\, e^{i\varphi_0} \cdot$$

$$\frac{\exp\{\lambda[\zeta\sqrt{1+r^2e^{i2\varphi_0}} + i(y-\eta)re^{i\varphi_0}]\}}{1 - K_o/\lambda}$$

$$= -\int_0^{\infty} dr e^{i\varphi_0} \cdot \frac{\exp\{\lambda\zeta\sqrt{1+r^2e^{i2\varphi_0}}\} \cdot}{\exp\{i(y-\eta)r\cos\varphi_0\} \cdot \exp\{-(y-\eta)r\sin\varphi_0\}}$$

$$\frac{}{1 - \frac{K_o}{\lambda}\sqrt{1 + r^2e^{i2\varphi_0}}}$$

$$\to 0 \quad (\text{as } y\to\infty)$$

Applying the Cauchy's integral theorem, then

$$\mathrm{P.V.}\int_0^{\infty} F(t)dt = -\pi i \frac{(\lambda/K_o)^2}{\sqrt{(\lambda/K_o)^2 - 1}} \cdot$$

$$\exp\{\lambda[\zeta(\lambda/K_o) + i(y-\eta)\sqrt{(\lambda/K_o)^2 - 1}]\},$$

that is

$$\int_0^{\pi/2} d\theta\, e^{\frac{\lambda}{\cos\theta}\zeta} \frac{\lambda\cos[\lambda(y-\eta)\tan\theta]}{(\lambda - K_o\sec\theta)\cos^2\theta}$$

$$= \pi(\frac{\lambda}{K_o})^2 \cdot e^{K_o\zeta(\lambda/K_o)^2} \cdot \frac{\sin[\lambda(y-\eta)\sqrt{(\lambda/K_o) - 1}]}{\sqrt{(\lambda/K_o)^2 - 1}}.$$

Appendix C Determinaton of the Constants f_o and ε for the Truncation Correction

It is convenient to express the asymptotic wave profile in equation (20) as

$$f = \frac{f_o}{\sqrt{K_ox}}\cos(K_ox + \varepsilon) \equiv \frac{C_1\cos K_ox + C_2\sin K_ox}{\sqrt{K_ox}},$$

where $f_o = (C_1^2 + C_2^2)^{\frac{1}{2}}$, and $\varepsilon = \tan^{-1}(-C_2/C_1)$.

Assume that there are n wave-height data points H_i, $i = 1, \ldots n$ before the truncation point for extrapolation, and let

$$f_i = \frac{C_1\cos(K_oX_i)}{\sqrt{K_oX_i}} + \frac{C_2\sin(K_oX_i)}{\sqrt{K_oX_i}},$$

$$S \equiv \sum_{i=1}^{n}(f_i - H_i).$$

Applying the least square method,

$$\frac{\partial S}{\partial C_1} = \sum_{i=1}^{n}(f_i - H_i)\frac{\cos(K_oX_i)}{\sqrt{K_oX_i}} = 0,$$

$$\frac{\partial S}{\partial C_2} = \sum_{i=2}^{n}(f_i - H_i)\frac{\sin(K_oX_i)}{\sqrt{K_oX_i}} = 0,$$

then

$$C_1\left[\sum_{i=1}^{n}\frac{\cos^2K_oX_i}{K_oX_i}\right] + C_2\left[\sum_{i=1}^{n}\frac{\cos K_oX_i\cdot\sin K_oX_i}{K_oX_i}\right]$$

$$= \sum_{i=1}^{n}\frac{H_i\cos K_oX_i}{\sqrt{K_oX_i}}$$

$$C_2\left[\sum_{i=1}^{n}\frac{\cos K_oX_i\cdot\sin K_oX_i}{K_oX_i}\right] + C_2\left[\sum_{i=1}^{n}\frac{\sin K_oX_i}{K_oX_i}\right]$$

$$= \sum_{i=1}^{n}\frac{H_i\sin K_oX_i}{\sqrt{K_oX_i}}$$

Solving the above linear algebraic equation, one may obtain C_1 and C_2, and finally the constants f_o and ε.

Appendix D Derivation of the Integrals of Asymptotic Wave Term in Equation (21)

The integrals of asymptotic wave term in equation (21) are

$$\int_M^\infty f_o \frac{\cos(KoX+\varepsilon)}{\sqrt{KoX}} \cos(KoX\sec\theta)dx + i\int_M^\infty f_o \frac{\cos(koX+\varepsilon)}{\sqrt{KoX}} \sin(KoX\sec\theta)\,dx$$

$$=\int_M^\infty f_o \frac{\cos(KoX+\varepsilon)}{\sqrt{KoX}} \exp(iKoX\sec\theta)\,dx$$

Let $x = \bar{t}^2/K_o$, then the above equation can be rewritten as

$$\frac{f_o}{Ko}\int_{\sqrt{MK_o}}^\infty [\, e^{i(\bar{t}^2+\varepsilon)} + e^{i(\bar{t}^2+\varepsilon)}\,] \cdot e^{i\bar{t}^2\sec\theta}\,d\bar{t}$$

$$=\frac{fo}{Ko}\int_{\sqrt{MKo}}^\infty (\cos\varepsilon + i\sin\varepsilon)\{\cos[(\sec\theta+1)\bar{t}^2] + i\sin[(\sec\theta+1)\bar{t}^2]\}d\bar{t}$$

$$+\frac{fo}{Ko}\int_{\sqrt{MKo}}^\infty (\cos\varepsilon - i\sin\varepsilon)\{\cos[(\sec\theta-1)\bar{t}^2] + i\sin[(\sec\theta-1)\bar{t}^2]\}d\bar{t}$$

$$=\frac{fo}{Ko}\{\cos\varepsilon\cdot\int_{\sqrt{MKo}}^\infty \cos[(\sec\theta+1)\bar{t}^2]\,d\bar{t} + \cos\varepsilon\cdot\int_{\sqrt{MKo}}^\infty \cos[(\sec\theta-1)\bar{t}^2]\,d\bar{t} - \sin\varepsilon\cdot\int_{\sqrt{MKo}}^\infty \sin[(\sec\theta+1)\bar{t}^2]\,d\bar{t} + \sin\varepsilon\cdot\int_{\sqrt{MKo}}^\infty \sin[(\sec\theta-1)\bar{t}^2]\,d\bar{t}\}.$$

Changing the integral variables once more by letting $\bar{t} = \frac{1}{\sqrt{(\sec\theta\pm1)}}\sqrt{\frac{\pi}{2}}\,t$, then the above equation

$$=\sqrt{\frac{\pi}{2}}\frac{fo}{Ko}\{\frac{\cos\varepsilon}{\sqrt{\sec\theta-1}}\int_{\sqrt{MKo(\sec\theta+1)}\sqrt{\frac{2}{\pi}}}^\infty \cos(\tfrac{\pi}{2}t^2)\,dt + \frac{\cos\varepsilon}{\sqrt{\sec\theta-1}}\int_{\sqrt{MKo(\sec\theta-1)}\sqrt{\frac{2}{\pi}}}^\infty \cos(\tfrac{\pi}{2}t^2)\,dt$$

$$-\frac{\sin\varepsilon}{\sqrt{\sec\theta-1}}\int_{\sqrt{MKo(\sec\theta+1)}\sqrt{\frac{2}{\pi}}}^\infty \sin(\tfrac{\pi}{2}t^2)\,dt + \frac{\sin\varepsilon}{\sqrt{\sec\theta-1}}\int_{\sqrt{MKo(\sec\theta-1)}\sqrt{\frac{2}{\pi}}}^\infty \sin(\tfrac{\pi}{2}t^2)\,dt$$

$$+i\sqrt{\frac{\pi}{2}}\frac{fo}{Ko}\{\frac{\cos\varepsilon}{\sqrt{\sec\theta+1}}\int_{\sqrt{MKo(\sec\theta+1)}\sqrt{\frac{2}{\pi}}}^\infty \sin(\tfrac{\pi}{2}t^2)\,dt + \frac{\cos\varepsilon}{\sqrt{\sec\theta-1}}\int_{\sqrt{MKo(\sec\theta-1)}\sqrt{\frac{2}{\pi}}}^\infty \sin(\tfrac{\pi}{2}t^2)\,dt$$

$$+\frac{\sin\varepsilon}{\sqrt{\sec\theta+1}}\int_{\sqrt{MKo(\sec\theta+1)}\sqrt{\frac{2}{\pi}}}^\infty \cos(\tfrac{\pi}{2}t^2)\,dt - \frac{\sin\varepsilon}{\sqrt{\sec\theta-1}}\int_{\sqrt{MKo(\sec\theta-1)}\sqrt{\frac{2}{\pi}}}^\infty \cos(\tfrac{\pi}{2}t^2)\,dt\}$$

$$=\sqrt{\frac{\pi}{2}}\frac{fo}{Ko}\{\frac{\cos\varepsilon}{\sqrt{\sec\theta+1}}[\frac{1}{2}-\int_0^{\sqrt{MKo(\sec\theta+1)}\sqrt{\frac{2}{\pi}}}\cos(\tfrac{\pi}{2}t^2)\,dt] + \frac{\cos\varepsilon}{\sqrt{\sec\theta-1}}[\frac{1}{2}-\int_0^{\sqrt{MKo(\sec\theta-1)}\sqrt{\frac{2}{\pi}}}\cos(\tfrac{\pi}{2}t^2)\,dt]$$

$$-\frac{\sin\varepsilon}{\sqrt{\sec\theta+1}}[\frac{1}{2}-\int_0^{\sqrt{MKo(\sec\theta+1)}\sqrt{\frac{2}{\pi}}}\sin(\tfrac{\pi}{2}t^2)\,dt] + \frac{\sin\varepsilon}{\sqrt{\sec\theta-1}}[\frac{1}{2}-\int_0^{\sqrt{MKo(\sec\theta-1)}\sqrt{\frac{2}{\pi}}}\sin(\tfrac{\pi}{2}t^2)\,dt]\}$$

$$+i\sqrt{\frac{\pi}{2}}\frac{fo}{Ko}\{\frac{\cos\varepsilon}{\sqrt{\sec\theta+1}}[\frac{1}{2}-\int_0^{\sqrt{MKo(\sec\theta+1)}\sqrt{\frac{2}{\pi}}}\sin(\tfrac{\pi}{2}t^2)\,dt] + \frac{\cos\varepsilon}{\sqrt{\sec\theta-1}}[\frac{1}{2}-\int_0^{\sqrt{MKo(\sec\theta-1)}\sqrt{\frac{2}{\pi}}}\sin(\tfrac{\pi}{2}t^2)\,dt]$$

$$+\frac{\sin\varepsilon}{\sqrt{\sec\theta+1}}[\frac{1}{2}-\int_0^{\sqrt{MKo(\sec\theta+1)}\sqrt{\frac{2}{\pi}}}\cos(\tfrac{\pi}{2}t^2)\,dt] - \frac{\sin\varepsilon}{\sqrt{\sec\theta-1}}[\frac{1}{2}-\int_0^{\sqrt{MKo(\sec\theta-1)}\sqrt{\frac{2}{\pi}}}\cos(\tfrac{\pi}{2}t^2)\,dt]\}.$$